

www.acsami.org Research Article

Camphene-Assisted Fabrication of Free-Standing Lithium-Ion Battery Electrode Composites

Jason A. Weeks, Samantha Lauro, James N. Burrow, Han Xiao, Joshua P. Pender, Adrian K. Rylski, Hugh Daigle, Zachariah Page, Christopher J. Ellison,* and C. Buddie Mullins*

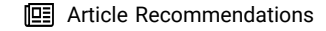


Cite This: ACS Appl. Mater. Interfaces 2022, 14, 45240–45253



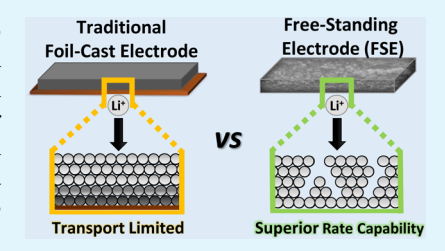
ACCESS I

III Metrics & More



s Supporting Information

ABSTRACT: Free-standing electrode (FSE) architectures hold the potential to dramatically increase the gravimetric and volumetric energy density of lithium-ion batteries (LIBs) by eliminating the parasitic dead weight and volume associated with traditional metal foil current collectors. However, current FSE fabrication methods suffer from insufficient mechanical stability, electrochemical performance, or industrial adoptability. Here, we demonstrate a scalable camphene-assisted fabrication method that allows simultaneous casting and templating of FSEs comprising common LIB materials with a performance superior to their foil-cast counterparts. These porous, lightweight, and robust electrodes simultaneously enable enhanced rate performance by



improving the mass and ion transport within the percolating conductive carbon pore network and eliminating current collectors for efficient and stable Li⁺ storage (>1000 cycles in half-cells) at increased gravimetric and areal energy densities. Compared to conventional foil-cast counterparts, the camphene-derived electrodes exhibit ~1.5× enhanced gravimetric energy density, increased rate capability, and improved capacity retention in coin-cell configurations. A full cell containing both a free-standing anode and cathode was cycled for over 250 cycles with greater than 80% capacity retention at an areal capacity of 0.73 mA h/cm². This active-material-agnostic electrode fabrication method holds potential to tailor the morphology of flexible, current-collector-free electrodes, thus enabling LIBs to be optimized for high power or high energy density Li⁺ storage. Furthermore, this platform provides an electrode fabrication method that is applicable to other electrochemical technologies and advanced manufacturing methods.

KEYWORDS: lithium-ion, batteries, lithium iron phosphate, lithium nickel manganese cobalt oxide, lithium titanate electrodes, composites, flexibility

1. INTRODUCTION

Since the early 1990s, lithium-ion batteries (LIBs) have been utilized as a convenient, reliable, and economically feasible source of portable energy storage. 1,2 Rapid technological advancements have enabled the near ubiquitous use of LIBs in consumer products such as laptops and cell phones, and further improvements hold potential to unlock the widespread adoption of emerging applications (i.e., electric vehicles and grid storage). With an ever-growing list of applications and the societal push toward decarbonization, the LIB market is projected to approach 3.0 TW h by 2030 (~4× the 2020's energy demand).3 Despite the commercial success of LIBs, further innovations at the material, cell, and system level are needed to meet the stringent requirements for these emerging applications (e.g., higher energy density, fast-charging ability, levelized cost of energy storage) and satiate the growing international energy demand.

The most extensive efforts to improve the performance of LIBs have focused on the intrinsic chemistry, via the electrolytes, 4-10 binders, 11-14 anodes, 15-18 and cathode materials. 19-26 However, only incremental changes in the cell chemistry (e.g., increasing Ni content in cathode; increased Si loading in blended anodes with graphite) have found

commercial success over the past decade. The slow commercial progress of new chemistries dictates the need for alternative electrode and cell designs that can enhance battery performance. At the electrode level, current LIBs utilize copper and aluminum current collectors (CCs) to mechanically support the anode and cathode films and provide connection to external circuitry. While these substrates are easily manufactured and inexpensive, the metal foils take up a considerable weight (approximately 10 and 6 wt % for the copper and aluminum, respectively, comprising 16% of the total cell weight) and volume fraction (approximately 9 and 6% of the cathode and anode, respectively) of the battery and reduce the achievable cell-level gravimetric energy density.²⁷⁻²⁹ Furthermore, the limited flexibility of the CC often restricts the design space of applications requiring lithium-ion storage devices and has confined the possibilities of new innovations in sectors

Received: May 10, 2022 Accepted: September 16, 2022 Published: September 29, 2022





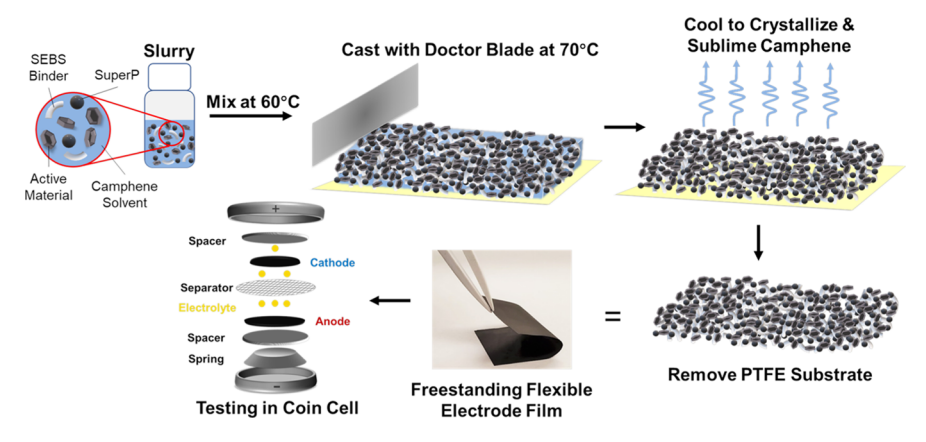


Figure 1. Schematic of the synthetic process of camphene-assisted fabrication of FSEs.

such as flexible-hybrid electronics. These limitations have inspired efforts to replace metal foil CCs with conductive, conformable, and lightweight alternatives such as carbon nanotubes, ^{30–35} nanowires, ^{36–38} reduced graphene oxide, ^{39–41} textile-based supports, ^{42,43} metal foam CCs, ^{44–46} and cross-linked carbon-based scaffolds. 47,48 These alternatives have demonstrated competitive electrochemical performance but do not yet provide a practical route toward commercialization due to complex and expensive processing requirements.

Other studies have shown the possibility to completely eliminate CCs by fabricating free-standing electrodes (FSEs). 31,44,49-55 Many metal-foil-free CCs have previously been produced using a variety of active materials and manufacturing methods, including slurry-casting on glass, 56 high-pressure/high-temperature filtration, 49,57 and 3D printing. 54,58 Unfortunately, most of these FSEs suffer from low specific capacities due to poor accessibility of active materials or insufficient electronic conductivities through the scaffolding matrix. Cathode active materials are currently the most expensive components of LIB electrodes and therefore must be fully utilized to obtain commercial viability. While preliminary work with FSEs shows great promise, further progress is required to generate mechanically robust FSE architectures that simultaneously avoid detrimental Ohmic and concentration overpotentials related to electronic/ionic conductivity and transport.

Alongside challenges related to material performance, another major bottleneck to the implementation of new battery technologies industrially is the upheaval of previous infrastructure and methodology. Large-scale changes to equipment, manufacturing lines, and training personnel are undesirable and costly. Herein, we introduce a camphenebased system for fabricating slurry cast FSEs using techniques analogous to the present roll-to-roll LIB electrode fabrication process (Figure 1) where electrodes are cast onto a substrate, dried, and then directly used in LIB cells. Camphene, which has a modest melting point (52 °C), high vapor pressure (3.4 mmHg @ 25 °C), and dendritic crystallization morphology, 59 has been shown to solubilize/disperse various polymers and particles 60-64 and most recently poly(styrene-block-ethylene/ butylene-block-styrene) block copolymers.⁶⁵ Due to these unique physical properties, when camphene is employed as an alternative solvent for slurry casting battery materials, the subsequent solidification of camphene crystallites doubles as a template to induce a percolating conductive network of battery electrode components. Direct removal of the camphene by sublimation via room temperature vacuum drying and subsequent delamination from the casting substrate results in the production of a porous, free-standing, and flexible composite electrode.

In the remainder of this paper, we demonstrate the ability of this synthetic platform to generate mechanically robust and flexible electrodes for LIBs. Performance testing of these composites illustrates their attractive properties and energy storage capabilities; for example, lithium-iron phosphate-based electrodes demonstrated stable electrochemical (de-)lithiation for over 1000 cycles with only small capacity losses (16 mA h/ g or 13%). All of the camphene-assisted FSEs demonstrate competitive to superior electrochemical capabilities when compared to analogous films cast on metal foil CCs and enable a ~50% increase in gravimetric capacity while maintaining superior rate capability in coin cell configurations. The improved rate capabilities can be attributed to the increased Li+ transport from the camphene templated structure. The demonstrated improvements suggest similar fabrication techniques can be utilized to improve the achievable energy density of LIBs. Additionally, the FSE electrode architecture provides improvements to other electrochemical applications such as other metal ion batteries, capacitors, fuel cells, electrolyzers, and capacitive desalination cells.

2. EXPERIMENTAL SECTION

2.1. Materials. All chemicals were used without further purification or treatment, unless stated otherwise. Lithium hexafluorophosphate (LiPF₆, 99.99%), diethyl carbonate (DEC, 99%), camphene (95%, MQ 100), toluene (>99.8%), and polystyrene-blockpoly(ethylene-ran-butylene)-block-polystyrene (SEBS, average M_w ~118,000, MQ 100, [S/EB, 29:71 mol/mol]) binder were obtained from Sigma-Aldrich. The Super P conductive additive, polyvinylidene fluoride binder (PVDF, >99.5%), lithium titanate (LTO, Li₄Ti₅O₁₂, >98%, D_{range} 0.2–10 μ m, D_{50} 0.9–1.8 μ m), lithium cobalt oxide (LCO, LiCoO₂, >98%, D_{range} 0.3–30 μ m, D_{50} 10–14 μ m), lithium iron phosphate (LFP, carbon-coated LiFePO₄, D_{range} 1–15 μ m, D_{50} $2.5-4.5 \mu m$), and lithium nickel manganese cobalt oxide (NMC811, LiNi $_{1.44~0.8}$ Co $_{0.1}$ Mn $_{0.1}$ O $_2$, 99%, $D_{\rm range}$ 5–45 μ m, D_{50} 9–15 μ m) were acquired from MTI Corporation. N-Methyl-2-pyrrolidone (NMP, >99%) was obtained from Tokyo Chemical Industry Co., Ltd. (TCI). 100 μ m thick Li foil (99.9%) was purchased from Alfa Aesar. Fluoroethylene carbonate (FEC, +99%) was obtained from Solvay. Celgard 2400 microporous monolayer membranes (polypropylene, 25 μm) were generously provided by Celgard.

2.2. FSE Fabrication. FSE films were manufactured through an altered slurry casting protocol, where camphene (M.P. = 51.5 °C) was

employed as the liquid solvent system by maintaining temperatures of approximately 65 °C throughout processing, except when the electrode is finally solidified by cooling at room temperature. Slurry solutions employed a 3:1 weight ratio of camphene/slurry solids (active material, binder, and conductive additive). The solid composition of the slurries consisted of an 85:10:5 weight ratios of active material/Super P/SEBS binder for all electrode composites with the exception of the LTO electrodes, which employed an 80:10:10 formulation. Upon the introduction of solids into the liquid camphene, the solutions mixed for 1 h in a 65 °C water bath.

Slurry solutions were cast utilizing a TMAX JK-TMJ-200 heated film coater with a doctor blade set to a film height of approximately 150 μ m. Films were hot-cast onto a polytetrafluoroethylene (Teflon, 0.001" thick) substrate and then immediately quenched by moving the sheet onto a chilled stainless-steel plate. Once the camphene solidified, films were dried under vacuum for 10 min. The resulting films were manually delaminated from the PTFE substrates, resulting in FSE films, and then dried under vacuum overnight to assure the removal of residual camphene. Electrode films were typically cast to an 18 in. \times 3 in. area.

In order to balance the capacities of the negative and positive electrodes used in the FSE LTO//LFP full cell, LTO electrodes used in this experiment were cast at a higher height using a bar set to 200 μ m. This resulted in films with higher mass loadings that could be used to balance the negative to positive capacity (N/P) ratio of the full cell. The capacities of the electrodes were determined using the active loading and the nominal capacity as detailed in Table S1. Full physical properties of the electrodes used in the full cell configuration are listed in Table S4.

- 2.3. Control Electrode Fabrication. Foil-cast control electrode films employed an analogous method to the composite electrodes above. Foil-cast control electrodes were fabricated using toluene or NMP as casting solvents when using SEBS and PVDF binders, respectively. The solid composition of the slurries consisted of an 85:10:5 weight ratio of active material/Super P/polymer binder for all electrodes with the exception of the LTO electrodes, which employed an 80:10:10 formulation. Slurry solutions were then cast using a doctor blade set to a height of 200 or 125 μm to fabricate the thick and thin control electrodes, respectively. Slurries were cast onto 12 um thick aluminum foil at room temperature for all active materials. Electrode films were dried for 2 h at 120 °C and ambient pressure to evaporate the majority of the solvent and then under vacuum to drive off remaining solvent overnight. Traditionally, LTO can be cast on either a copper or aluminum CC. All LTO control electrodes used in this study employed an aluminum foil CC to lower the impact of inactive weight on the control cells and provide a more representative comparison.
- **2.4. Material Characterization.** X-ray diffraction (XRD) patterns were acquired through a Rigaku Miniflex 600 diffractometer utilizing Cu K α radiation ($\lambda = 1.5418$ Å) from 5 to 80° in a continuous scan mode (1° min⁻¹) with a step width of $2\theta = 0.02^{\circ}$. Scanning electron micrographs (SEMs) were taken using a Thermo Fisher Quanta 650 environmental scanning electron microscope with an applied accelerating voltage of 30 kV. X-ray photoelectron spectroscopy (XPS) spectra were recorded using a monochromated 120 W Al Kal X-ray source ($h\nu$ = 1486.5 eV). Four-point probe measurements were conducted with a manual four-point resistivity probe (Lucas S302; Lucas Laboratories). Full instrumental specifications and experimental parameters can be found in the Supporting
- 2.5. Electrode Preparation. Circular free-standing and foil-cast control electrodes were punched directly from the electrode films with a TMAX die electrode punch to a diameter of 13 and 15 mm for anodes and cathodes, respectively. Thicknesses of the resulting electrodes were measured using an IP65 Digimatic micrometer.
- 2.6. Electrochemical Analysis. Electrochemical properties of the FSE composites were analyzed in half-cell configurations using 2032 coin-type cells versus lithium foil (Alfa Aesar). Full cell batteries utilizing a LFP cathode and a LTO anode (N/P ratio = 1.26:1) were also tested to elucidate the practicality of the composite system. All

cells were assembled using a Celgard 2400 polymer membrane and an electrolyte composed of 1 M lithium hexafluorophosphate (LiPF₆) in FEC/DEC (1:1 by volume) solution. Excess electrolyte was used (>5 drops) to flood the cell and provide sufficient wetting. Cycling performance and cyclic voltammetry (CV) tests were conducted using a multichannel battery test system (BT 2043, Arbin). Electrochemical potential windows were adjusted to the optimal range of each electrode material employed. The electrochemical window for each configuration demonstrated in this paper is as follows: (1) LFP versus Li/Li⁺, 2.5-4.0 V; (2) LCO versus Li/Li⁺, 3.0-4.2 V; (3) NCM811 versus Li/Li⁺, 2.7-4.3 V; (4) LTO versus Li/Li⁺, 1.0-2.5 V; and (5) LFP versus LTO, 0.9-2.6 V. Full details about the electrochemical cycling conditions can be found in the Supporting Information (Table S1). The electrochemical data presented is an average of three identical cells to assure reproducibility in the results.

3. RESULTS AND DISCUSSION

3.1. Chemical Stability Testing. To probe the compatibility of camphene with the electroactive materials, XRD and XPS were used to analyze the chemical status of the active materials before and after camphene exposure. Results from XRD (shown in Figure S1) suggest that even excessive soaking of the various active materials in hot liquid camphene for 6 h did not affect the bulk chemical composition of these active materials.

Furthermore, XPS was employed to determine the chemical impact of camphene exposure on the electroactive material surfaces. Survey scans of the electrode materials and their respective composites (Figures S2 and S3) depicted the expected elemental compositions for each active material composition without noticeable contamination. High-resolution region scans (Figures S4-S7) of the pristine active materials and the as-formed FSE composites indicated no significant chemical change in the active materials. It should be noted that pristine nickel cobalt manganese oxide (NCM) and LTO materials contained a significant titanium oxide and cobalt oxide contamination, respectively, on their surface. These impurities were likely present due to the incomplete reaction of the precursor materials during synthesis. Region scans of the FSE composites denote a removal of these contaminants, suggesting that the electrode fabrication process simulated an additional washing step and removed some of the surface level precursor contamination during the composite formation of NCM and LTO. Overall, these results demonstrate that camphene did not detrimentally react with or alter the chemical composition of the active materials in the final composite, confirming the chemically agnostic nature of the fabrication technique. Full details on the chemical stability testing and resulting analysis can be found in the Supporting Information of this document.

3.2. FSE Films. To demonstrate the versatility of the camphene solvent system, we fabricated FSEs using multiple electroactive materials, including LFP, LTO, LCO, and NCM811, thereby testing the utility of the FSE platform under a diverse set of operating conditions. LFP cathodes are known for their extensive cycle-life (>80% capacity retention @ 1000 s of cycles at high rate and depth-of-discharge) and therefore served as a prime candidate to test long-term stability. Due to the large lithiation potentials of NCM811 and the reactive Ni and Mn constituents, the high voltage stability was probed to elucidate chemical compatibility of camphene with oxidizing materials. LTO tests both the compatibility of the camphene-assisted fabrication route with nanoparticulate materials and the anodic capability of the resulting composites.

Additionally, due to the well-studied and stable nature of these materials, analysis of the effects of the FSE architecture could be decoupled from active material degradation during battery cycling.

Electrodes employing these electroactive materials were produced using typical slurry casting method conducted at elevated temperatures using a camphene: solids ratio of 3:1. Full experimental procedures for the fabrication of these FSE films can be found in Experimental Section 2.2 and the Supporting Information. A representative FSE film formed from the camphene casting process is pictured in Figure 2a.

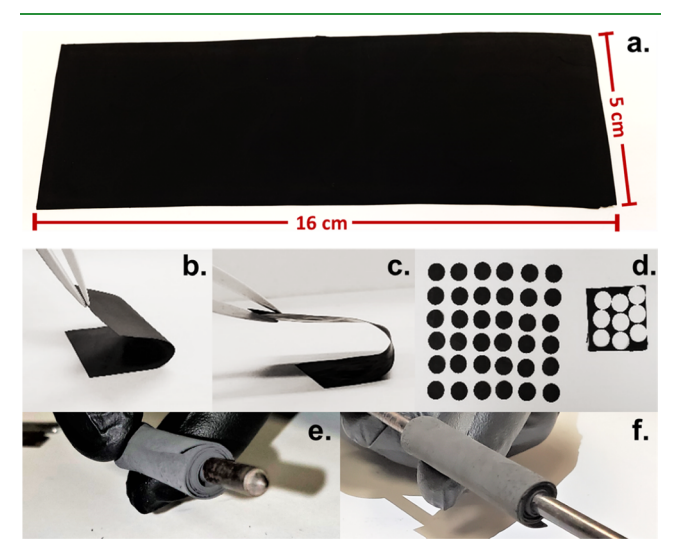


Figure 2. Photographs of FSE films. (a) Whole FSE film after delamination from Teflon substrate. Flexibility and mechanical integrity of FSE demonstrated in (b,c). Electrodes punched directly from the FSE film to 13 mm diameter disks shown in (d). Practicality for length scale configurations was tested by wrapping the FSEs around a 4 mm rod. Photos depict the electrodes in a jellyroll orientation from the side (e) and areal (f) perspective, respectively.

The mechanical stability of the FSE films is important for their implementation in roll-to roll processing, as the films will need to be able to withstand processing into a stacked or wound cell configuration.⁶⁶ Figure 2b,c depicts the exceptional ability of the FSE films to be bent and punched into electrodes without notable mechanical degradation (i.e., no cracks or creases). To demonstrate the FSE compatibility with practical length scale configurations (i.e., cylindrical, prismatic), Figure 2e,f demonstrates the film rolled numerous times around a 4 mm cylinder. These results exhibit the ability of the FSE films to overcome the physical limitations of traditional foil-cast electrode films that would typically crease or crack upon folding or bending. Typical PVDF binder containing electrodes that have limited flexibility and tend to crack and delaminate from the CC, resulting in disconnection of the electroactive layer and loss of usable energy/power⁶⁷ Compatibility with standard processing methods makes this synthesis platform attractive from a manufacturing perspective, as no major changes to the current industrial infrastructure are required for implementation.

After fabricating FSEs comprising NCM, LFP, LCO, and LTO, scanning electron microscopy was employed for closer inspection of film homogeneity, material distribution, and camphene-induced pore morphology (Figure 3). Crosssections of these electrodes (Figure 3a,e,i,m) exhibited a relatively flat and uniform structure. As visible in Figure 3d,h,l,p, the active materials are anchored in the conductive composite electrode architecture by SEBS polymer coated with Super P. The casting process results in two different electrode faces, one which was in contact with the Teflon substrate during casting (denoted as the "substrate side", Figure 3b,f,j,n) and one which maintained exposure to vacuum (denoted as "vacuum side", Figure 3c,g,k,m). With the exception of nanoparticulate LTO, where settling effects likely resulted in a denser vacuum side (Figure 30) and more porous substrate side (Figure 3n), little difference in morphology between the two electrode faces was observed. Relative to traditional NMP foil-cast electrode films (Figure S17), the FSE films

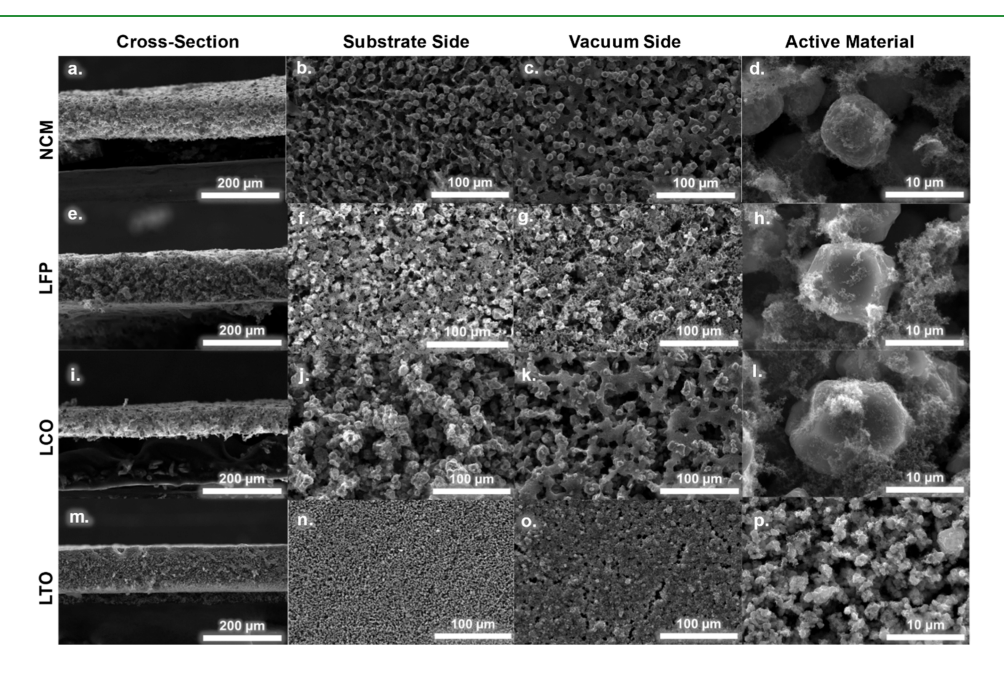


Figure 3. Scanning electron microscopy images of FSE films consisting of NCM811 (a-d), LFP (e-h), LCO (i-l), and LTO (m-p). The film cross section (a,e,i,m), substrate-exposed face (b,f,j,n), vacuum-exposed face (c,g,k,o), and imbedded active material particles (d,h,l,p) are shown for each active material composition with scale bars of 200, 100, 100, and 10 μ m, respectively.

Table 1. Physical Properties of the FSE Electrodes Analyzed for C-2 Cycling in This Study

electrode	total mass (mg)	active mass (mg)	thickness (μm)	porosity (%)	electrode area (cm²)	areal loading (mg/cm²)
NCM811-1	10.48	8.91	115	65	1.33	6.70
NCM811-2	9.46	8.04	118	69	1.33	6.05
LFP-1	10.10	8.58	107	62	1.33	6.45
LFP-2	10.60	9.01	105	59	1.33	6.77
LCO-1	9.82	8.35	110	69	1.33	6.28
LCO-2	8.90	7.57	100	69	1.33	5.69
LTO-1	10.55	8.44	112	75	1.33	6.35
LTO-2	12.49	9.99	166	80	1.33	7.51

Table 2. Physical Properties of the Foil-Cast Control Electrodes Analyzed for C-2 Cycling in This Study alongside the Physical Properties of the Aluminum Current Collector of the Controls

electrode	total mass (mg)	active mass (mg)	thickness (μm)	porosity (%)	electrode area (cm²)	areal loading (mg/cm²)
NCM811-thin-1	6.78	5.75	45	42	1.33	4.32
NCM811-thin-2	6.75	5.73	47	44	1.33	4.31
NCM811-thick-1	11.43	9.71	70	37	1.33	7.30
NCM811-thick-2	11.01	9.35	68	37	1.33	7.03
LFP-thin-1	6.02	5.10	42	42	1.33	3.83
LFP-thin-2	6.03	5.11	40	43	1.33	3.84
LFP-thick-1	10.78	9.15	71	38	1.33	6.88
LFP-thick-2	10.55	8.96	68	37	1.33	6.74
LCO-thin-1	7.21	6.13	49	50	1.33	4.61
LCO-thin-2	7.11	6.04	50	51	1.33	4.54
LCO-thick-1	13.96	11.86	85	44	1.33	8.92
LCO-thick-2	14.13	12.00	84	42	1.33	9.02
LTO-thin-1	6.93	5.49	41	55	1.33	4.13
LTO-thin-2	6.92	5.50	41	55	1.33	4.13
LTO-thick-1	11.82	9.45	118	73	1.33	7.11
LTO-thick-2	11.78	9.40	89	65	1.33	7.07
aluminum CC	5.54	N/a	12	N/a	1.33	N/a

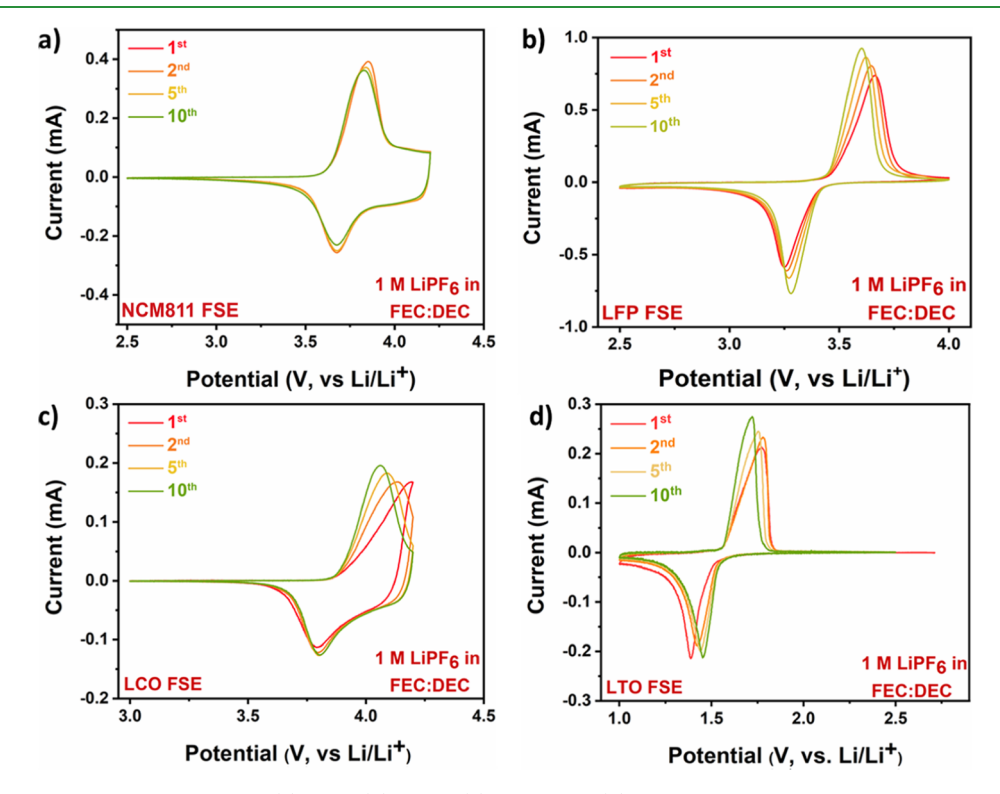


Figure 4. Cyclic voltammograms of NCM811 (a), LFP (b), LCO (c), and LTO (d) and FSE composites vs lithium foil.

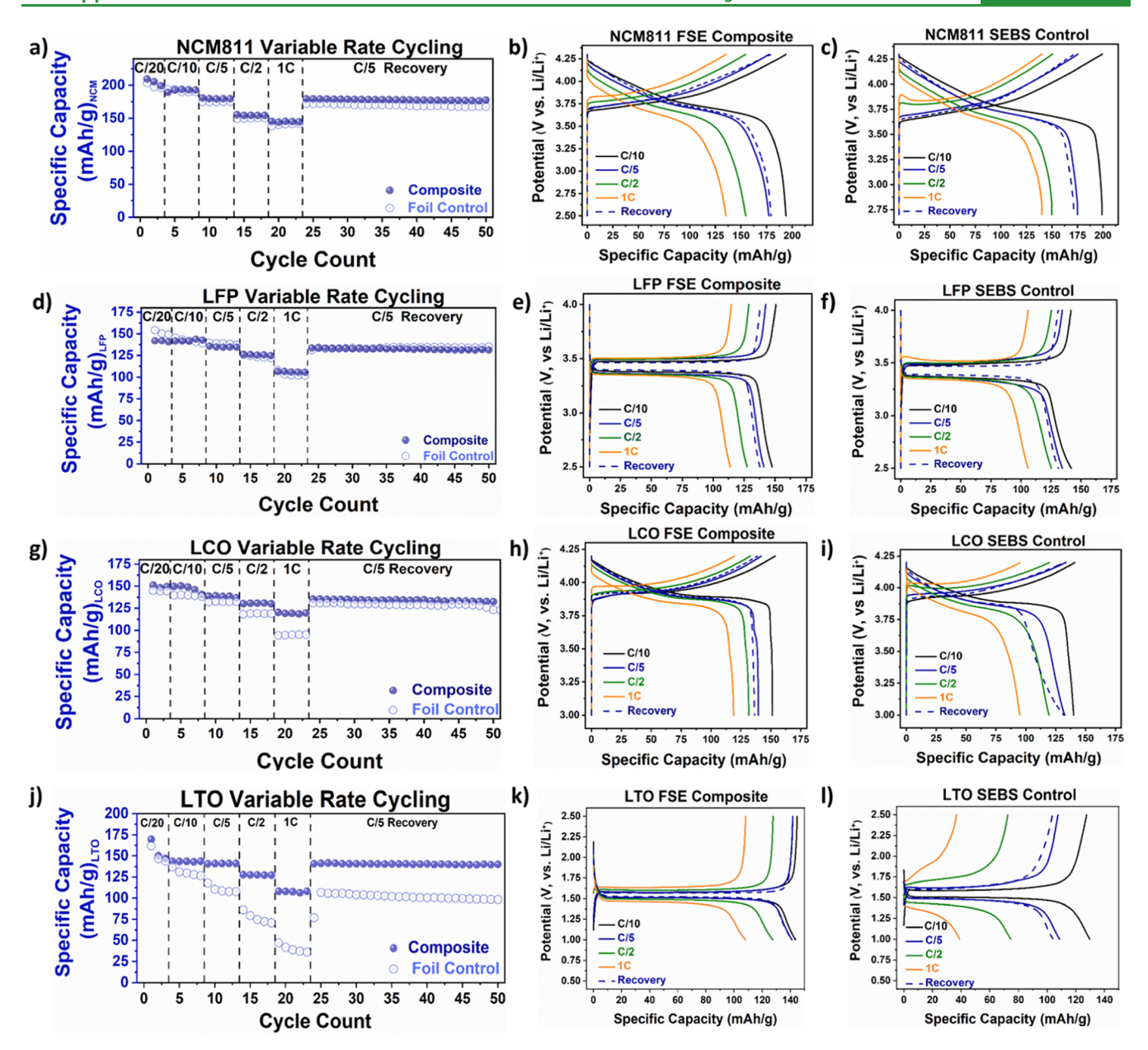


Figure 5. Rate capability performance testing of the camphene-assisted FSEs and foil-cast controls. Variable rate cycling and resulting chargedischarge curves, respectively, of the NCM811 (a-c), LFP (d-f), LCO (g-i), and LTO (j-l) half-cells.

demonstrate a more clearly defined pore structure and overall higher porosity. This is supported by density-based calculations (Tables 1 and 2) revealing a ~20% increase in porosity of FSEs compared to foil-cast electrodes, which can decrease mass transport limitations via enhanced electrolyte penetration.

3.3. Electrochemical Activity. Electrochemical activity and performance metrics of the FSE composites were evaluated versus two controls: (1) foil-cast electrodes with lower active mass loading [thin controls] and (2) foil-cast electrodes with comparable active mass loading [thick controls]. The morphology and structure of foil-cast electrodes are dependent on the settling nature of particles after casting and due to the intrinsic nature of this morphology, and the thickness of LIB electrodes is limited to approximately 100-150 μ m to ensure sufficient lithium storage kinetics and mechanical stability. Therefore, thinly cast electrodes with lower active mass loadings were fabricated to establish a baseline for ideal electrochemical kinetics and performance.

On the other hand, for electrode-level analyses, the electroactive layer thickness is crucial in drawing fair comparisons; control electrodes with lower electroactive mass loading will inherently demonstrate a larger fraction of inactive electrode mass from the metallic CC, and electrodes with similar volumetric active material loading (mg/cm³) that have different thicknesses will display different areal capacities. As such, controls were also fabricated with comparable electroactive mass loadings on foil to enable valid quantification of the benefits of the FSE system to enhance the electrode-level performance of LIBs. Full information about the FSEs and control electrodes' physical properties are listed in Tables 1 and 2, respectively.

As previously mentioned, battery performance without an external CC is contingent upon electrochemical stability, conductivity, and active material accessibility. Before investigating the propensity for Li⁺ storage in these FSE composites, four-point probe analysis was conducted to quantify the bulk

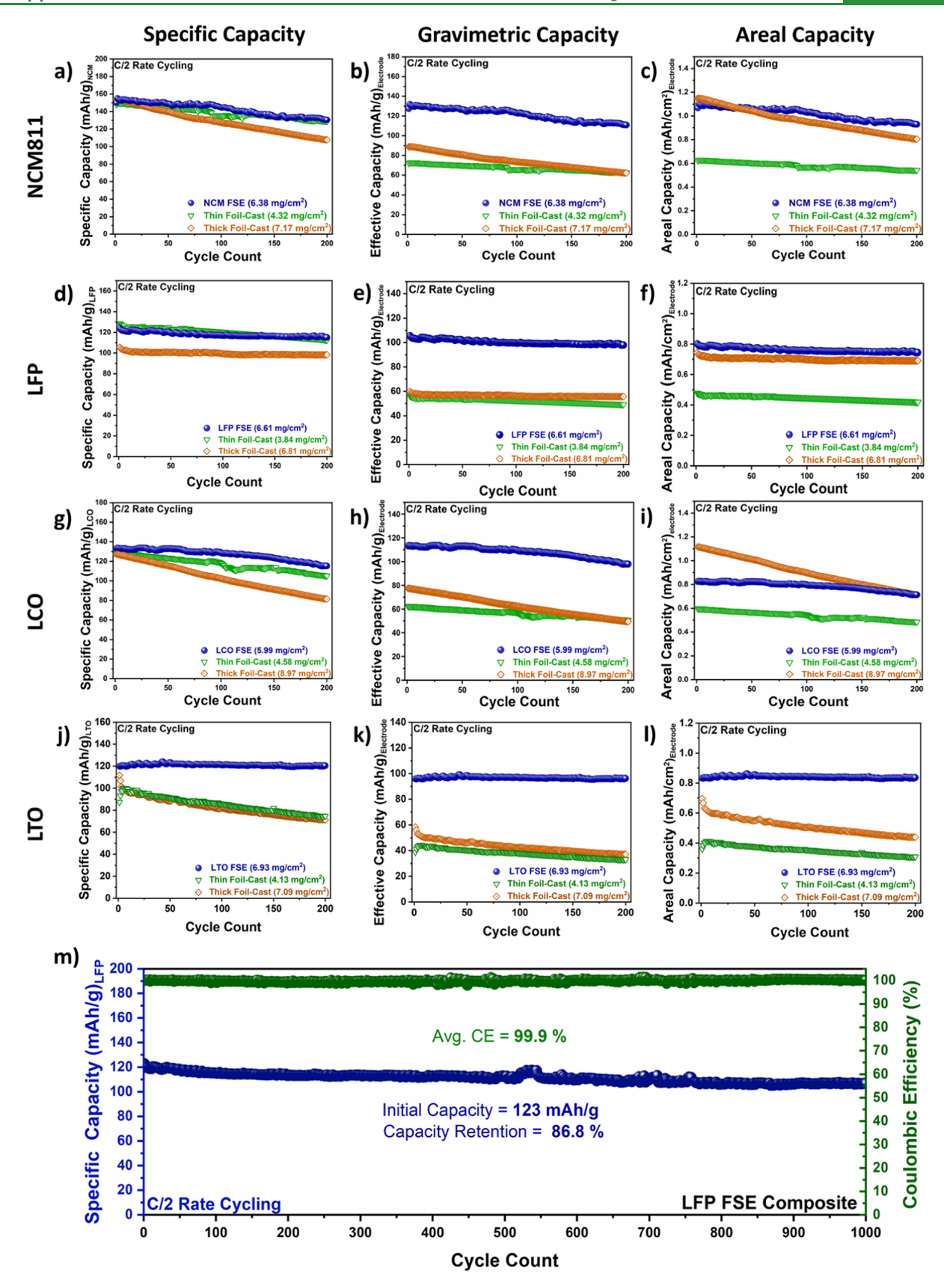


Figure 6. Comparative long-term performance testing of the NCM811 (a–c), LFP (d–f), LCO (g–i), and LTO (j–l) FSE electrodes with their foil-cast counterparts at a C/2 rate for 200 cycles. A comparative analysis was conducted for the cells' specific capacity (a,d,g,j), electrode gravimetric capacity (b,e,h,k), and areal capacity (c,f,i,l). Extensive lifetime cycling was conducted on the LFP-based composite (m) to demonstrate the stability of the camphene-assisted FSE system.

conductivity of each respective FSE. The sheet conductivities of all the FSEs were approximately 0.1 S/cm irrespective of active material (Table S2), which is above the threshold required for high-rate, low overpotential electrochemical cycling.⁶⁸ This similarity in conductivity suggests the electrical conductivity is primarily attributed to the homogeneous dispersion of the conductive Super P additive throughout the FSEs. The slight variation in conductivity between FSEs comprised different active materials points toward the versatility of this camphene-assisted FSE fabrication process for use with diverse materials.

The electrochemical activity of the FSE composites was investigated via CV in half-cells with a scan rate of 0.1 mV/s in 1 M LiPF₆ FEC/DEC electrolyte solution (Figure 4). Upon cycling, the NCM811 FSE displayed peaks between 3.6 and 4.0 V in Figure 4a, indicative of the expected Ni⁴⁺/Ni³⁺ and Ni³⁺/ Ni²⁺ redox reactions. The LFP-, LCO-, and LTO-based composites (Figure 4b,c,d) show reversible (de)lithiation peaks centered at 3.4, 3.9, and 1.5 V, respectively. The slight activation process observed for these materials, where initial cycles required a slightly increased overpotential for Li+ removal/insertion, was likely related to the stabilization of interfaces and/or structural reorganization within these early cycles. Overall, these CV experiments revealed that the FSE composites displayed very comparable electrochemical behavior to their foil-cast counterparts (Figure S8), demonstrating electrochemical accessibility for Li+ storage of the active materials within these composite matrices.

After investigating the potential-dependence of the Li⁺ insertion processes for the various active material composites, variable (dis)charging current densities were applied in halfcells to quantify the rate performance of the FSE electrodes (Figure 5) in comparison to their thin foil-cast counterparts (Figures S12 and S13). Low-rate (C/20) electrochemical cycling revealed near identical specific capacities between the composite and control electrodes on an active material basis. With the exception of LFP, the FSEs exhibited a slight increase in specific capacity for all of the electrode materials at slow rate (de)lithiation, confirming that the camphene-assisted FSE configuration provides full accessibility of active materials throughout the composite in the absence of ionic transport limitations. In contrast, intentionally introducing transportinduced limitations to the cells via higher-rate cycling (1 C) demonstrated the benefits of the conductive and porous FSE architecture, as an improvement in specific capacity (4 mA h/g for NCM, 3 mA h/g for LFP, 25 mA h/g for LCO, and 58 mA h/g for LTO) was observed for all electrode materials compared to conventional foil-cast counterparts with thinner electroactive thicknesses. As a result, the FSEs demonstrated overall larger rate retention (i.e., percent capacity achieved at 1 C compared to the nominal C/20 capacity) of 70.8 versus 70.3% for NCM, 79.8 versus 65.3% for LCO, 74.8 versus 68.4% for LFP, and 62.3 versus 26.6% for LTO for FSEs versus foil-cast counterparts, respectively.

While the composite architecture clearly does not fully eliminate transport limitations, these CC-free FSEs exhibited a significant improvement in rate capability as compared to conventional foil-cast cells. Further results of this variable rate testing emphasized the robust nature of the FSEs, which showed exceptional capacity recovery at C/5 for all materials (≥99.0% compared to ≤99.0% for foil-cast controls) after high-rate (de)lithiation. Comparisons between the FSEs and the thin foil-cast electrodes were used to emphasize how the

camphene-generated pore structure assists with mass transport limitations even in contrast to electrochemically ideal or thin film electrodes. Full comparison of variable rate cycling between all electrodes can be found in Table S5.

Battery electrode performance can be limited by factors irrespective of the intrinsic properties of individual active materials, which create parasitic overpotentials related to insufficient electronic conductivity and/or mass transport limitations. Accordingly, charge-discharge curves helped to draw further insights into the enhancement of rate performance of the FSEs (Figure 5) compared to foil-cast electrodes (Figure S10). In half-cells of these active materials that have well-defined, energetically similar lithiation sites, Ohmic overpotentials from ionic or electronic resistivity manifest as the difference in plateau voltage on the charge and discharge branches of the cycle. On the other hand, concentration overpotentials result in the sloping region at larger states of (dis)charge as the Li⁺ concentration profile becomes the ratelimiting factor for the (de)lithiation process. In a set voltage window, variation in either of these factors will affect the practically achievable Li+-storage capacity.

Comparing the voltage gaps between the charge and discharge profiles from cycling at rates of C/10 to 1 C demonstrated that the FSEs exhibited lower Ohmic overpotentials than their foil-cast counterparts (change in plateau voltage of 30 vs 60 mV, 80 vs 170 mV, 100 vs 150 mV, and 220 vs 230 mV for FSEs vs foil-cast controls comprising LFP, LTO, LCO, and NCM, respectively). As the FSE and the foil-cast cells were fabricated with identical electrolyte formulations (i.e., with identical ionic conductivity), the smaller Ohmic overpotentials observed for the FSEs was likely instead related to an enhanced electronic conductivity in the FSEs, despite their larger porosity, compared to their foil-cast counterparts (Tables 1 and 2). Coupled with the fact that each set of electrodes comprised similar electroactive thicknesses and identical ratios of solid components, the lower observed Ohmic overpotentials in the FSEs suggested that the unique camphene-templating process led to the formation of a betterconnected conductive, percolating framework of Super P in contrast to the conventional foil-cast technique, where the resulting morphology relied instead on random particle mixing and settling. Additionally, compared to the discharge curves of foil-cast controls (Figure S10), discharge curves of the FSEs demonstrated larger slopes near full depth of discharge. These increased slopes were indicative of smaller concentration overpotentials and suggest a reduction of mass transport limitations throughout the porous FSE structure compared to the foil-cast control. Overall, these variable rate-cycling results suggested that the FSEs exhibited improved (de)lithiation kinetics due to more efficient transport of both electrons and ions in these porous 3D architectures compared to conventional electrodes, even in the absence of an external CC and when utilizing thicker electrodes containing higher active mass loadings.

3.4. Long-Term Cycling of FSE Composites. Constant current C/2 performance testing was employed to investigate the long-term stability of the FSEs in lithium-ion half-cells and compare their electrochemical properties to conventional foilcast systems. Figure 6 shows the values calculated for the specific capacity relating to the total amount of active material in the FSE (Figure 6a,d,g,j), the gravimetric capacity concerning the entire electrode mass including binder, conductive additive, and CCs (Figure 6b,e,h,k), and the areal

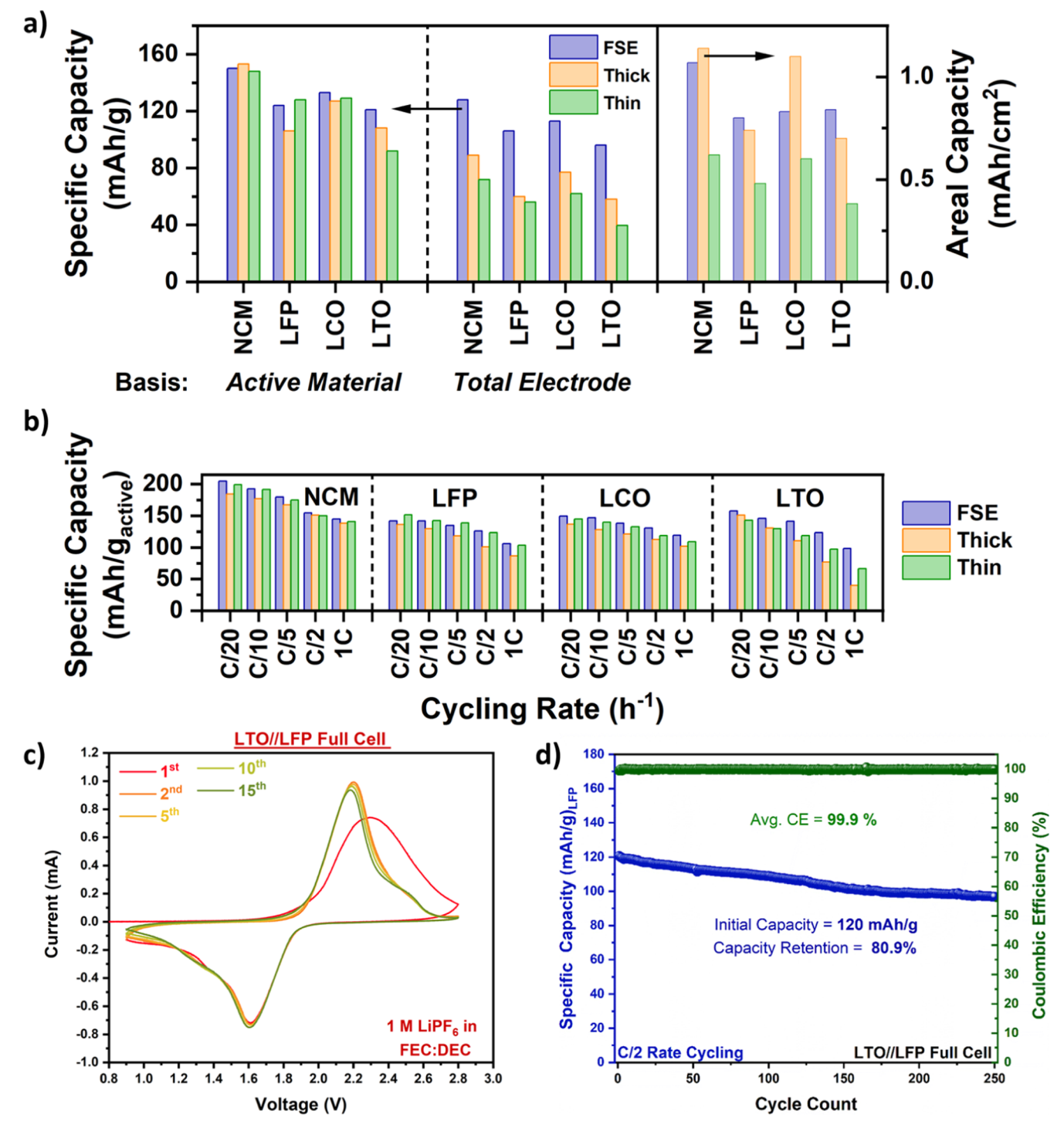


Figure 7. Summary for the electrochemical properties of the camphene-assisted FSE composites. (a) Variable C-rate and (b) capacity comparison 3D plot contrasting electrochemical metrics of the FSEs with the thin foil-cast electrodes. (c) CV of LTO/LFP full cell. (d) C/2 performance testing of LTO/LFP cell.

capacity (capacity provided per unit area cm⁻²) (Figure 6c,f,i,l).

As the rate-capability of FSEs showed promising results compared to controls, long-term C/2 cycling further demonstrated the potential for the camphene-template system to be used to fabricate stable, large energy density FSEs with comparable or superior Li⁺ storage ability compared to metal-foil counterparts. All FSEs successfully demonstrated stable galvanostatic lithiation/delithiation for 200 cycles with capacity

retention greater than 80%, verifying that the metal foil CC was not necessary to maintain long-term mechanical stability. The FSE materials demonstrated long-term capacity retentions that were greater than or equal to the control samples. Specifically, the NCM, LFP, LCO, and LTO FSEs delivered initial specific capacities of 150, 124, 133, and 121 mA h/g, with capacity retentions of 87.1, 93.1, 86.5, and 99.9% capacity retention at 200 cycles, respectively. On the other hand, the NCM, LFP, LCO and LTO thin foil-cast controls provided

initial specific capacities of 148, 128, 129, and 92 mA h/g, with capacity retentions of 86.9, 87.6, 81.3, and 81.1%, respectively. The NCM, LFP, LCO, and LTO thick foil-cast controls provided initial specific capacities of 153, 106, 127, and 108 mA h/g, with capacity retentions of 70.3, 90.9, 64.2, and 65.9%, respectively. Comparing the cells on a per active material basis highlights the potential of the camphenetemplated architecture to provide comparable specific capacity and capacity retention to the electrochemically ideal thin controls, while hosting $\sim 1.5 \times$ the amount of active material. Furthermore, comparing the FSEs to the thick controls elucidates their mechanically robust nature as noted by their significantly increased capacity retentions.

In commercial LIBs, the copper foil and aluminum foil CCs make up approximately 35 and 15% of the electrode mass of the anode and cathode, respectively.²⁷ Improvement in the achievable specific capacity on an active material basis alongside enhanced long-term stability shows promise for the FSEs to bring about considerable improvements to LIBs on the electrode level due to the concurrent elimination of the dead weight and volume of the metallic CC. When comparing with metal foil control films of similar areal loading of active material, the overall electrode gravimetric capacity was significantly improved for all active materials investigated here. The NCM, LFP, LCO, and LTO FSEs demonstrated 44, 76, 46, and 65% increases in effective capacity, respectively, even compared to their thick foil-cast counterparts due in large part to the elimination of the dense metal foil CCs enabled by the camphene-assisted fabrication procedure. Similar improvements were denoted in the areal capacities of the FSE composites. The NCM, LFP, LCO, and LTO FSEs provided areal capacities of 1.07, 0.80, 0.83, and 0.84 mA h/cm², providing improvements of 73, 67, 38, and 121%, respectively, compared to the thin-cast control. Even comparing the FSEs to the thick-cast controls (higher areal loadings), the LFP and LTO composites provided a greater areal capacity (0.80 vs 0.74 mA h/cm² and 0.84 vs 0.70 mA h/cm², respectively) due to their superior rate capabilities. While having lower initial areal capacities, the NCM and LCO FSEs depicted higher end of life areal capacities (0.93 vs 0.80 mA h/cm² and 0.72 vs 0.71 mA h/cm², respectively) due to their enhanced capacity retention. A full summary of the results obtained from the C/2 long-term cycling can be found in Table S6.

By performing these experiments against two sets of control electrodes, one with lower active mass loading and one with comparable loading, we can draw valid comparisons to electrochemical performance and capacity metrics of the FSEs. Electrochemical assessment of the FSE composites in a coin cell configuration confirmed that superior electrochemical kinetics and long-term stability can be achieved from films without metal foil support and higher areal mass loadings using this camphene-assisted fabrication process.

Additionally, as LFP is known for its outstanding stability and cycle life, extreme long-term cycling (1000 cycles) was performed for this FSE (Figure 6m) to further elucidate any effects the FSE system may have on electrode stability. The LFP FSEs maintain average Coulombic efficiencies of 99.99% over the 1000 cycles with a final capacity retention of 86.8%. These systems have excellent long-term stability and dramatic increases in the overall gravimetric electrode capacity, proving that the camphene-assisted FSE design could be a viable pathway toward scalable fabrication of larger energy density batteries.

Overall, the half-cell electrochemical performance of the composites demonstrated the material-agnostic capability of the camphene-assisted route to create high energy density FSEs. Variable rate cycling and extensive long-term performance testing of these electrodes suggested that the threedimensional, porous structure of the electrodes permitted better rate capability for lithiation and a stable host for longterm cycling. Additional testing of foil-cast controls using a traditional NMP solvent and PVDF binder was conducted to mimic commercial electrodes. Cycling data for these electrodes can be found in (Figures S12 and S13). For further details on control electrode fabrication and composition, please refer to the Experimental Section.

3.5. Full Cell Compatibility Testing. While half-cell performance testing displays exceptional electrochemical activity, lithium-half cells provide the composites with a near-infinite source of lithium during cycling. In contrast, for a real world LIB, depletion of lithium inventory in the cell is one of the most common causes of battery failure and performance degradation over time. Therefore, full-cell configurations were fabricated to elucidate performance metrics of FSEs in a

Due to their long-term stability and single feature voltage profiles, LTO and LFP were chosen as a respective cathode and anode pair. Mimicking the protocol of previous literature and experimentation, full cells utilized a N/P ratio of 1.26:1 and underwent constant current-constant voltage formation cycles at C/20 before long-term testing was conducted. 69,70 Cyclic voltammograms of the LTO/LFP cell (Figure 7c) suggested that a 0.9-2.6 V voltage window was sufficient to achieve 100% depth of (dis)charge upon cycling. Subsequent voltammograms depicted similar performance to the half-cell configurations, where after an initial activation during the 1st cycle, reversible lithiation processes occurred.

Overall, the full cell configuration of these FSEs provided an electrochemical performance that mirrored the individual halfcell counterparts, as shown in Figure 7d. Even without traditional metal foil CCs, these systems achieved an initial charge capacity of 120 mA h/g on a cathode material basis, with a capacity retention of 80.9% and an average Coulombic efficiency of 99.95% after 250 cycles at an areal loading of 0.73 mA h/cm². These results suggest that the camphene-assisted FSEs act as stable hosts for lithium-storage materials even after extensive lithiation/delithiation.

The capacity retention of the FSE full cells suggested that the electrodes maintained their mechanical integrity even after extensive cycling. For confirmation, cells were disassembled and electrodes were retrieved for post-mortem analysis. These electrodes displayed very little mechanical adherence to the polymer separator, and after simple electrode recovery with forceps, macroscopic visual inspection denoted little to no physical change after cycling. The flexibility of the electrodes, tested after a simple ethanol wash and drying, was nearly identical to pre-cycled FSEs (Figure S14). One of the major bottlenecks to the effective recycling of battery separators is that electrode materials are commonly physically embedded into the separator after extensive cycling.²⁷ Therefore, these FSEs may provide a route toward more easily recycled materials in LIB systems. Post-mortem microscopic inspection of the FSE electrodes (Figure S15) depicted that, while typical foil-cast electrodes (Figure S16) demonstrated a major reduction in distinguishable features due to particle pulverization and the formation of interface layers, the FSEs retained a

majority of their discernible features. This is likely due to the porous nature of the composites, providing void volume to compensate any volumetric changes induced from lithiation/delithiation. The integrity of physical properties and structural composition elucidates how the full cell composed of a pair of FSEs is able to undergo stable (de)lithiation for more than 250 cycles.

4. CONCLUSIONS

In this study, we demonstrated a new pathway for fabricating free-standing LIB electrodes using readily available, cheap, and non-toxic camphene as a dual-purpose solvent that crystalizes to provide a pore template. We demonstrated the ability of the camphene-template to develop porous, conductive architectures that improve the high-rate (de)lithiation performance over more than 200 cycles with multiple electroactive materials. Comparative electrochemical analysis of various types of foil-cast controls suggest that this hierarchical structure provided both higher electrode energy density and improved rate capability due to the simultaneous elimination of heavy metal-foil CCs and the camphene-templated pore structure, which provided better electrochemical accessibility to the active materials. Compared to traditional electrode fabrication which relies on solution-based settling of active materials, the solid-state templating nature of the crystallizing camphene casting solution promotes the growth of a porous, structurally defined composite electrode. While the composite structure demonstrates superior rate capabilities, the additional porosity resulted in lower volumetric capacity. Future studies will seek to quantify the effects of different material compositions, variable slurry cast heights, and mechanical tuning of porosity through calendaring to better understand how camphene-templated electrode characteristics affect electrochemical performance. With this knowledge, optimized electrode designs can be formed.

We think that the fundamental understanding of these unique electrode architectures could provide valuable information for how electrode engineering can alleviate the constraints of current generation lithium-ion battery technology such as energy density, rate capability, and accessible recycling. In addition to better rate capabilities and gravimetric energy densities, the FSE composites maintained mechanical integrity throughout cycling and were able to be reclaimed intact post-mortem. Simple mechanical delamination of the FSEs from the separator after cycling could promote straightforward recycling efforts for these electrodes in the future. While these attributes make FSEs an enticing electrode design for future LIB configurations, future work will evaluate if the thermally and electronically conducting support can be successfully implemented into large scale cell designs such as multi-layer pouch, cylindrical, and prismatic cells.

Overall, this synthetic platform provides significant electrode-level improvements to conventional systems while employing a fabrication technique that is compatible with continuous roll-to-roll processing, as well as other advanced manufacturing methods such as mold-casting, thermoforming, and 3D printing. If coupled with advancements in active material and electrolyte chemistries, this scalable and adjustable electrode fabrication process can assist in reaching the energy density targets required for next generation LIB energy storage devices.

ASSOCIATED CONTENT

Supporting Information

The Supporting Information is available free of charge at https://pubs.acs.org/doi/10.1021/acsami.2c08143.

XRD of pristine and camphene-soaked active materials, XPS of pristine active materials and FSE composites, charge—discharge curves of the control and FSE electrodes, four-point probe analysis of the electrical conductivity of the control and FSE electrodes, cyclic voltammograms of SEBS and PVDF controls, tabulated physical properties of the FSE and control electrodes, tabulated electrochemical performance metrics of the FSE and control electrodes, post-mortem micrographs of the foil-cast controls and FSE composites, comparative cycling for PVDF and SEBS foil cast controls, mercury intrusion porosimetry results of the LTO and LFP composites, SEMs of the foil-cast controls, EIS of the LFP//LFP FSE cell, and mechanical performance metrics of LFP and LFP composites (PDF)

AUTHOR INFORMATION

Corresponding Authors

Christopher J. Ellison – Department of Chemical Engineering and Materials Science, The University of Minnesota, Minneapolis, Minnesota 55455, United States; oorcid.org/0000-0002-0393-2941; Email: cellison@umn.edu

C. Buddie Mullins — Department of Chemistry, The University of Texas at Austin, Austin, Texas 78712-1224, United States; John J. McKetta Department of Chemical Engineering, The University of Texas at Austin, Austin, Texas 78712-1589, United States; Texas Materials Institute, The University of Texas at Austin, Austin, Texas 78712-1591, United States; orcid.org/0000-0003-1030-4801; Email: mullins@che.utexas.edu

Authors

Jason A. Weeks — Department of Chemistry, The University of Texas at Austin, Austin, Texas 78712-1224, United States; orcid.org/0000-0003-0335-6128

Samantha Lauro — Department of Chemistry, The University of Texas at Austin, Austin, Texas 78712-1224, United States; orcid.org/0000-0003-4771-9795

James N. Burrow – John J. McKetta Department of Chemical Engineering, The University of Texas at Austin, Austin, Texas 78712-1589, United States; ⊚ orcid.org/0000-0002-7445-3788

Han Xiao – Department of Chemical Engineering and Materials Science, The University of Minnesota, Minneapolis, Minnesota 55455, United States

Joshua P. Pender – Department of Chemistry, The University of Texas at Austin, Austin, Texas 78712-1224, United States Adrian K. Rylski – Department of Chemistry, The University of Texas at Austin, Austin, Texas 78712-1224, United States

Hugh Daigle – Petroleum and Geosystems Engineering, The University of Texas at Austin, Austin, Texas 78712-1589, United States

Zachariah Page – Department of Chemistry, The University of Texas at Austin, Austin, Texas 78712-1224, United States

Complete contact information is available at: https://pubs.acs.org/10.1021/acsami.2c08143

Author Contributions

The manuscript was written through equal contributions of all authors. All authors have given approval to the final version of the manuscript.

Notes

The authors declare no competing financial interest.

ACKNOWLEDGMENTS

The authors gratefully acknowledge the Welch Foundation [grant F-1436 (C.B.M.) and F-2007 (Z.P.)], National Science Foundation via a Partnerships for Innovation grant [PFI-1940986 (C.B.M.)], Zsolt Rumy Innovation Chair (C.J.E.), and National Science Foundation via CAREER [grant no. DMR-2045336 (A.K.R. and Z.P.)] for supporting this work. The authors also thank Celgard for generously supplying membrane separators and Solvay for providing FEC.

REFERENCES

- (1) Brandt, K. Historical Development of Secondary Lithium Batteries. *Solid State Ionics* **1994**, *69*, 173–183.
- (2) Schipper, F.; Aurbach, D. A Brief Review: Past, Present and Future of Lithium Ion Batteries. *Russ. J. Electrochem.* **2016**, *52*, 1095–1121.
- (3) Energy Storage Grand Challenge Energy Storage Market Report; U.S. Department of Energy, 2020; p 65.
- (4) Lau, J.; DeBlock, R. H.; Butts, D. M.; Ashby, D. S.; Choi, C. S.; Dunn, B. S. Sulfide Solid Electrolytes for Lithium Battery Applications. *Adv. Energy Mater.* **2018**, *8*, 1800933.
- (5) Wang, F.; Borodin, O.; Ding, M. S.; Gobet, M.; Vatamanu, J.; Fan, X.; Gao, T.; Eidson, N.; Liang, Y.; Sun, W.; Greenbaum, S.; Xu, K.; Wang, C. Hybrid Aqueous/Non-Aqueous Electrolyte for Safe and High-Energy Li-Ion Batteries. *Joule* **2018**, *2*, 927–937.
- (6) Tan, D. H. S.; Wu, E. A.; Nguyen, H.; Chen, Z.; Marple, M. A. T.; Doux, J.-M.; Wang, X.; Yang, H.; Banerjee, A.; Meng, Y. S. Elucidating Reversible Electrochemical Redox of Li6PSSCl Solid Electrolyte. *ACS Energy Lett.* **2019**, *4*, 2418–2427.
- (7) Chen, J.; Fan, X.; Li, Q.; Yang, H.; Khoshi, M. R.; Xu, Y.; Hwang, S.; Chen, L.; Ji, X.; Yang, C.; He, H.; Wang, C.; Garfunkel, E.; Su, D.; Borodin, O.; Wang, C. Electrolyte Design for LiF-Rich Solid–Electrolyte Interfaces to Enable High-Performance Microsized Alloy Anodes for Batteries. *Nat. Energy* **2020**, *5*, 386–397.
- (8) Haregewoin, A. M.; Wotango, A. S.; Hwang, B.-J. Electrolyte Additives for Lithium Ion Battery Electrodes: Progress and Perspectives. *Energy Environ. Sci.* **2016**, *9*, 1955–1988.
- (9) Xue, W.; Gao, R.; Shi, Z.; Xiao, X.; Zhang, W.; Zhang, Y.; Zhu, Y. G.; Waluyo, I.; Li, Y.; Hill, M. R.; Zhu, Z.; Li, S.; Kuznetsov, O.; Zhang, Y.; Lee, W.-K.; Hunt, A.; Harutyunyan, A.; Shao-Horn, Y.; Johnson, J. A.; Li, J. Stabilizing Electrode—Electrolyte Interfaces to Realize High-Voltage LillLiCoO2 Batteries by a Sulfonamide-Based Electrolyte. *Energy Environ. Sci.* 2021, 14, 6030—6040.
- (10) Hubble, D.; Brown, D. E.; Zhao, Y.; Fang, C.; Lau, J.; McCloskey, B. D.; Liu, G. Liquid Electrolyte Development for Low-Temperature Lithium-Ion Batteries. *Energy Environ. Sci.* **2022**, *15*, 550–578.
- (11) Gonçalves, R.; Oliveira, J.; Silva, M. P.; Costa, P.; Hilliou, L.; Silva, M. M.; Costa, C. M.; Lanceros-Méndez, S. Poly(Styrene–Butene/Ethylene–Styrene): A New Polymer Binder for High-Performance Printable Lithium-Ion Battery Electrodes. ACS Appl. Energy Mater. 2018, 1, 3331–3341.
- (12) Jiao, X.; Yin, J.; Xu, X.; Wang, J.; Liu, Y.; Xiong, S.; Zhang, Q.; Song, J. Highly Energy-Dissipative, Fast Self-Healing Binder for Stable Si Anode in Lithium-Ion Batteries. *Adv. Funct. Mater.* **2021**, *31*, 2005699.
- (13) Hu, S.; Wang, L.; Huang, T.; Yu, A. A Conductive Self-Healing Hydrogel Binder for High-Performance Silicon Anodes in Lithium-Ion Batteries. *J. Power Sources* **2020**, 449, 227472.

- (14) Chen, H.; Wu, Z.; Su, Z.; Chen, S.; Yan, C.; Al-Mamun, M.; Tang, Y.; Zhang, S. A Mechanically Robust Self-Healing Binder for Silicon Anode in Lithium Ion Batteries. *Nano Energy* **2021**, *81*, 105654.
- (15) Weeks, J. A.; Sun, H.-H.; Srinivasan, H. S.; Burrow, J. N.; Guerrera, J. V.; Meyerson, M. L.; Dolocan, A.; Heller, A.; Mullins, C. B. Facile Synthesis of a Tin Oxide-Carbon Composite Lithium-Ion Battery Anode with High Capacity Retention. *ACS Appl. Energy Mater.* **2019**, *2*, 7244–7255.
- (16) Jia, H.; Li, X.; Song, J.; Zhang, X.; Luo, L.; He, Y.; Li, B.; Cai, Y.; Hu, S.; Xiao, X.; Wang, C.; Rosso, K. M.; Yi, R.; Patel, R.; Zhang, J.-G. Hierarchical Porous Silicon Structures with Extraordinary Mechanical Strength as High-Performance Lithium-Ion Battery Anodes. *Nat. Commun.* **2020**, *11*, 1474.
- (17) Pender, J. P.; Guerrera, J. V.; Wygant, B. R.; Weeks, J. A.; Ciufo, R. A.; Burrow, J. N.; Walk, M. F.; Rahman, M. Z.; Heller, A.; Mullins, C. B. Carbon Nitride Transforms into a High Lithium Storage Capacity Nitrogen-Rich Carbon. *ACS Nano* **2019**, *13*, 9279–9291.
- (18) Zhang, K.; Zhang, Y.; Zhou, J.; Li, Y.; Zheng, B.; Yang, F.; Kai, Y. A Stress-Based Charging Protocol for Silicon Anode in Lithium-Ion Battery: Theoretical and Experimental Studies. *J. Energy Storage* **2020**, 32, 101765.
- (19) Voronina, N.; Sun, Y.-K.; Myung, S.-T. Co-Free Layered Cathode Materials for High Energy Density Lithium-Ion Batteries. *ACS Energy Lett.* **2020**, *5*, 1814–1824.
- (20) Manthiram, A. A Reflection on Lithium-Ion Battery Cathode Chemistry. *Nat. Commun.* **2020**, *11*, 1550.
- (21) Park, S.; Oh, J.; Kim, J. M.; Guccini, V.; Hwang, T.; Jeon, Y.; Salazar-Alvarez, G.; Piao, Y. Facile Preparation of Cellulose Nanofiber Derived Carbon and Reduced Graphene Oxide Co-Supported LiFePO4 Nanocomposite as Enhanced Cathode Material for Lithium-Ion Battery. *Electrochim. Acta* **2020**, 354, 136707.
- (22) Zhong, Z.; Chen, L.; Zhu, C.; Ren, W.; Kong, L.; Wan, Y. Nano LiFePO4 Coated Ni Rich Composite as Cathode for Lithium Ion Batteries with High Thermal Ability and Excellent Cycling Performance. *J. Power Sources* **2020**, *464*, 228235.
- (23) Zhu, L.; Bao, C.; Xie, L.; Yang, X.; Cao, X. Review of Synthesis and Structural Optimization of LiNi1/3Co1/3Mn1/3O2 Cathode Materials for Lithium-Ion Batteries Applications. *J. Alloys Compd.* **2020**, *831*, 154864.
- (24) Sun, H. H.; Dolocan, A.; Weeks, J. A.; Heller, A.; Mullins, C. B. Stabilization of a Highly Ni-Rich Layered Oxide Cathode through Flower-Petal Grain Arrays. *ACS Nano* **2020**, *14*, 17142–17150.
- (25) Park, G.-T.; Yoon, D. R.; Kim, U.-H.; Namkoong, B.; Lee, J.; Wang, M. M.; Lee, A. C.; Gu, X. W.; Chueh, W. C.; Yoon, C. S.; Sun, Y.-K. Ultrafine-Grained Ni-Rich Layered Cathode for Advanced Li-Ion Batteries. *Energy Environ. Sci.* **2021**, *14*, 6616–6626.
- (26) Park, G.-T.; Park, N.-Y.; Noh, T.-C.; Namkoong, B.; Ryu, H.-H.; Shin, J.-Y.; Beierling, T.; Yoon, C. S.; Sun, Y.-K. High-Performance Ni-Rich Li[Ni0.9—XCo0.1Alx]O2 Cathodes via Multi-Stage Microstructural Tailoring from Hydroxide Precursor to the Lithiated Oxide. *Energy Environ. Sci.* 2021, 14, 5084—5095.
- (27) Marshall, J.; Gastol, D.; Sommerville, R.; Middleton, B.; Goodship, V.; Kendrick, E. Disassembly of Li Ion Cells—Characterization and Safety Considerations of a Recycling Scheme. *Metals* **2020**, *10*, 773.
- (28) Li, H. Practical Evaluation of Li-Ion Batteries. *Joule* **2019**, 3, 911–914.
- (29) Harlow, J. E.; Ma, X.; Li, J.; Logan, E.; Liu, Y.; Zhang, N.; Ma, L.; Glazier, S. L.; Cormier, M. M. E.; Genovese, M.; Buteau, S.; Cameron, A.; Stark, J. E.; Dahn, J. R. A Wide Range of Testing Results on an Excellent Lithium-Ion Cell Chemistry to Be Used as Benchmarks for New Battery Technologies. *J. Electrochem. Soc.* 2019, 166, A3031.
- (30) Han, B. J.; Liu, T.; Huang, Z. J.; Chen, D. M.; Zhu, Y. S.; Zhou, C. Y.; Li, Y. S.; Yin, Y. H.; Wu, Z. P. Preparation of Flexible Carbon Nanotube Ropes for Low-Voltage Heat Generator. *Appl. Phys. Lett.* **2017**, *110*, 103902.

- (31) Agostini, M.; Lim, D. H.; Brutti, S.; Lindahl, N.; Ahn, J. H.; Scrosati, B.; Matic, A. Free-Standing 3D-Sponged Nanofiber Electrodes for Ultrahigh-Rate Energy-Storage Devices. *ACS Appl. Mater. Interfaces* **2018**, *10*, 34140–34146.
- (32) Liu, W.; Chen, Z.; Zhou, G.; Sun, Y.; Lee, H. R.; Liu, C.; Yao, H.; Bao, Z.; Cui, Y. 3D Porous Sponge-Inspired Electrode for Stretchable Lithium-Ion Batteries. *Adv. Mater.* **2016**, *28*, 3578–3583.
- (33) Zhu, L.; Peng, H.-J.; Liang, J.; Huang, J.-Q.; Chen, C.-M.; Guo, X.; Zhu, W.; Li, P.; Zhang, Q. Interconnected Carbon Nanotube/Graphene Nanosphere Scaffolds as Free-Standing Paper Electrode for High-Rate and Ultra-Stable Lithium—Sulfur Batteries. *Nano Energy* 2015, 11, 746—755.
- (34) Yuan, D.; Cheng, J.; Qu, G.; Li, X.; Ni, W.; Wang, B.; Liu, H. Amorphous Red Phosphorous Embedded in Carbon Nanotubes Scaffold as Promising Anode Materials for Lithium-Ion Batteries. *J. Power Sources* **2016**, *301*, 131–137.
- (35) Wu, Y.; Wang, J.; Jiang, K.; Fan, S. Applications of Carbon Nanotubes in High Performance Lithium Ion Batteries. *Front. Phys.* **2014**, *9*, 351–369.
- (36) Geng, X.; Rao, M.; Li, X.; Li, W. Highly Dispersed Sulfur in Multi-Walled Carbon Nanotubes for Lithium/Sulfur Battery. *J. Solid State Electrochem.* **2013**, *17*, 987–992.
- (37) Xing, Z.; Huang, C.; Deng, Y.; Zhao, Y.; Ju, Z. Encapsulating Silicon Nanoparticles into N-Doped Carbon Film as a High-Performance Anode for Lithium Ion Batteries. *Funct. Mater. Lett.* **2018**, *11*, 1850067.
- (38) Wang, H.-G.; Yuan, S.; Ma, D.-L.; Zhang, X.-B.; Yan, J.-M. Electrospun Materials for Lithium and Sodium Rechargeable Batteries: From Structure Evolution to Electrochemical Performance. *Energy Environ. Sci.* **2015**, *8*, 1660–1681.
- (39) Chen, Y.; Fu, K.; Zhu, S.; Luo, W.; Wang, Y.; Li, Y.; Hitz, E.; Yao, Y.; Dai, J.; Wan, J.; Danner, V. A.; Li, T.; Hu, L. Reduced Graphene Oxide Films with Ultrahigh Conductivity as Li-Ion Battery Current Collectors. *Nano Lett.* **2016**, *16*, 3616–3623.
- (40) Zhou, D.; Song, W.-L.; Li, X.; Fan, L.-Z. Hierarchical Porous Reduced Graphene Oxide/SnO2 Networks as Highly Stable Anodes for Lithium-Ion Batteries. *Electrochim. Acta* **2016**, 207, 9–15.
- (41) He, J.; Wang, N.; Yang, Z.; Shen, X.; Wang, K.; Huang, C.; Yi, Y.; Tu, Z.; Li, Y. Fluoride Graphdiyne as a Free-Standing Electrode Displaying Ultra-Stable and Extraordinary High Li Storage Performance. *Energy Environ. Sci.* **2018**, *11*, 2893–2903.
- (42) Jagdale, P.; Nair, J. R.; Khan, A.; Armandi, M.; Meligrana, G.; Hernandez, F. R.; Rusakova, I.; Piatti, E.; Rovere, M.; Tagliaferro, A.; Winter, M.; Gerbaldi, C. Waste to Life: Low-Cost, Self-Standing, 2D Carbon Fiber Green Li-Ion Battery Anode Made from End-of-Life Cotton Textile. *Electrochim. Acta* **2021**, 368, 137644.
- (43) Zolin, L.; Nair, J. R.; Beneventi, D.; Bella, F.; Destro, M.; Jagdale, P.; Cannavaro, I.; Tagliaferro, A.; Chaussy, D.; Geobaldo, F.; Gerbaldi, C. A Simple Route toward Next-Gen Green Energy Storage Concept by Nanofibres-Based Self-Supporting Electrodes and a Solid Polymeric Design. *Carbon* **2016**, *107*, 811–822.
- (44) Gwon, H.; Hong, J.; Kim, H.; Seo, D.-H.; Jeon, S.; Kang, K. Recent Progress on Flexible Lithium Rechargeable Batteries. *Energy Environ. Sci.* **2014**, *7*, 538–551.
- (45) Yu, J.; Dang, Y.; Bai, M.; Peng, J.; Zheng, D.; Zhao, J.; Li, L.; Fang, Z. Graphene-Modified 3D Copper Foam Current Collector for Dendrite-Free Lithium Deposition. *Front. Chem.* **2019**, *7*, 748.
- (46) Yang, G. F.; Song, K. Y.; Joo, S. K. A Metal Foam as a Current Collector for High Power and High Capacity Lithium Iron Phosphate Batteries. *J. Mater. Chem. A* **2014**, *2*, 19648–19652.
- (47) Pender, J. P.; Xiao, H.; Dong, Z.; Cavallaro, K. A.; Weeks, J. A.; Heller, A.; Ellison, C. J.; Mullins, C. B. Compact Lithium-Ion Battery Electrodes with Lightweight Reduced Graphene Oxide/Poly(Acrylic Acid) Current Collectors. ACS Appl. Energy Mater. 2019, 2, 905–912.
- (48) Ha, H.; Shanmuganathan, K.; Ellison, C. J. Mechanically Stable Thermally Crosslinked Poly(Acrylic Acid)/Reduced Graphene Oxide Aerogels. ACS Appl. Mater. Interfaces 2015, 7, 6220–6229.
- (49) Chew, S. Y.; Ng, S. H.; Wang, J.; Novák, P.; Krumeich, F.; Chou, S. L.; Chen, J.; Liu, H. K. Flexible Free-Standing Carbon

- Nanotube Films for Model Lithium-Ion Batteries. Carbon 2009, 47, 2976-2983.
- (50) Park, Y.; Park, G.; Park, J.; Lee, J. Robust Free-Standing Electrodes for Flexible Lithium-Ion Batteries Prepared by a Conventional Electrode Fabrication Process. *Electrochim. Acta* **2017**, 247, 371–380.
- (51) Gao, S.; Zhang, D.; Zhu, K.; Tang, J. A.; Gao, Z.; Wei, Y.; Chen, G.; Gao, Y. Flexible V2O3/Carbon Nano-Felts as Free-Standing Electrode for High Performance Lithium Ion Batteries. *J. Alloys Compd.* **2017**, 702, 13–19.
- (52) Zhang, P.; Wang, W.; Liu, J.; Zhou, C.; Zhou, J.-J.; Xu, L.; Chen, L. N-Doped Carbon-Wrapped Cobalt—Manganese Oxide Nanosheets Loaded into a Three-Dimensional Graphene Nanonetwork as a Free-Standing Anode for Lithium-Ion Storage. *ACS Appl. Nano Mater.* **2021**, *4*, 3619–3630.
- (53) Spencer, M. A.; Augustyn, V. Free-Standing Transition Metal Oxide Electrode Architectures for Electrochemical Energy Storage. *J. Mater. Sci.* **2019**, *54*, 13045–13069.
- (54) Kohlmeyer, R. R.; Blake, A. J.; Hardin, J. O.; Carmona, E. A.; Carpena-Núñez, J.; Maruyama, B.; Daniel Berrigan, J. D.; Huang, H.; Durstock, M. F. Composite Batteries: A Simple yet Universal Approach to 3D Printable Lithium-Ion Battery Electrodes. *J. Mater. Chem. A* 2016, 4, 16856–16864.
- (55) Zhou, G.; Li, F.; Cheng, H.-M. Progress in Flexible Lithium Batteries and Future Prospects. *Energy Environ. Sci.* **2014**, *7*, 1307–1338.
- (56) Park, Y.; Park, G.; Park, J.; Lee, J. Robust Free-Standing Electrodes for Flexible Lithium-Ion Batteries Prepared by a Conventional Electrode Fabrication Process. *Electrochim. Acta* **2017**, 247, 371–380.
- (57) Shah, R.; Gu, J.-Y.; Razzaq, A. A.; Zhao, X.; Shen, X.-W.; Miao, L.; Yan, C.-L.; Peng, Y.; Deng, Z. Freestanding Electrode Pairs with High Areal Density Fabricated under High Pressure and High Temperature for Flexible Lithium Ion Batteries. *ACS Appl. Energy Mater.* **2018**, *1*, 3171–3179.
- (58) Bao, Y.; Liu, Y.; Kuang, Y.; Fang, D.; Li, T. 3D-Printed Highly Deformable Electrodes for Flexible Lithium Ion Batteries. *Energy Storage Mater.* **2020**, *33*, 55–61.
- (59) Stull, D. R. Vapor Pressure of Pure Substances. Organic and Inorganic Compounds. *Ind. Eng. Chem.* **1947**, *39*, 517–540.
- (60) Araki, K.; Halloran, J. W. Porous Ceramic Bodies with Interconnected Pore Channels by a Novel Freeze Casting Technique. *J. Am. Ceram. Soc.* **2005**, *88*, 1108–1114.
- (61) Moon, Y. W.; Shin, K. H.; Koh, Y. H.; Choi, W. Y.; Kim, H. E. Porous Alumina Ceramics with Highly Aligned Pores by Heat-Treating Extruded Alumina/Camphene Body at Temperature near Its Solidification Point. *J. Eur. Ceram. Soc.* **2012**, *32*, 1029–1034.
- (62) Jen, H. K.; Chen, W.-L.; Chang, Y.-M.; Ke, C.-T. Gelation Behaviour of UHMWPE/Camphene. J. Mater. Sci. 1997, 32, 3607—3611.
- (63) Choi, J.-W.; Maeng, W.-Y.; Koh, Y.-H.; Lee, H.; Kim, H.-E. 3D Plotting Using Camphene as Pore-Regulating Agent to Produce Hierarchical Macro/Micro-Porous Poly(ε -Caprolactone)/Calcium Phosphate Composite Scaffolds. *Materials* **2019**, *12*, 2650.
- (64) Yang, M. C.; Perng, J. S. Camphene as a Novel Solvent for Polypropylene: Comparison Study Based on Viscous Behavior of Solutions. *J. Appl. Polym. Sci.* **2000**, *76*, 2068–2074.
- (65) Xiao, H. Synthesis of Porous Materials and Their Applications in Electrochemistry and Additive Manufacturing; Graduate School of the University of Minnesota, December 2020; p 193.
- (66) Meyer, C.; Bockholt, H.; HaseIrieder, W.; Kwade, A. Characterization of the Calendering Process for Compaction of Electrodes for Lithium-Ion Batteries. J. Mater. Process. Technol. 2017, 249, 172–178.
- (67) Amin-Sanayei, R.; He, W. Chapter 10—Application of Polyvinylidene Fluoride Binders in Lithium-Ion Battery. In *Advanced Fluoride-Based Materials for Energy Conversion*; Nakajima, T., Groult, H., Eds.; Elsevier, 2015; pp 225–235.

- (68) Tian, R.; Alcala, N.; O'Neill, S. J. K.; Horvath, D. V.; Coelho, J.; Griffin, A. J.; Zhang, Y.; Nicolosi, V.; O'Dwyer, C.; Coleman, J. N. Quantifying the Effect of Electronic Conductivity on the Rate Performance of Nanocomposite Battery Electrodes. ACS Appl. Energy Mater. 2020, 3, 2966-2974.
- (69) Keil, P.; Jossen, A. Charging Protocols for Lithium-Ion Batteries and Their Impact on Cycle Life—An Experimental Study with Different 18650 High-Power Cells. J. Energy Storage 2016, 6,
- (70) Zhu, J.; Dewi Darma, M. S.; Knapp, M.; Sørensen, D. R.; Heere, M.; Fang, Q.; Wang, X.; Dai, H.; Mereacre, L.; Senyshyn, A.; Wei, X.; Ehrenberg, H. Investigation of Lithium-Ion Battery Degradation Mechanisms by Combining Differential Voltage Analysis and Alternating Current Impedance. J. Power Sources 2020, 448,

Recommended by ACS

Expansion-Tolerant Lithium Anode with Built-In LiF-Rich Interface for Stable 400 Wh kg-1 Lithium Metal Pouch Cells

Ziqiang Liu, Xiayin Yao, et al.

II II V 18 2022

ACS MATERIALS LETTERS

READ **Z**

Self-Healing Silicon Anode via the Addition of GaInSn-**Encapsulated Microcapsules**

Jian Yang, Fang Wu, et al.

OCTOBER 10, 2022

ACS APPLIED ENERGY MATERIALS

READ

Epitaxial Metal-Organic Framework for Stabilizing the Formation of a Solid Electrolyte Interphase on the Si Anode of a Lithium-Ion Battery

Jaewook Shin, EunAe Cho, et al.

AUGUST 05, 2022

ACS SUSTAINABLE CHEMISTRY & ENGINEERING

READ [7

(3-Aminopropyl)triethoxysilane as an Electrolyte Additive for Enhancing the Thermal Stability of Silicon Anode in **Lithium-Ion Batteries**

Tian Tan, Denis Y. W. Yu, et al.

AUGUST 19, 2022

ACS APPLIED ENERGY MATERIALS

READ

Get More Suggestions >